Geometric analysis of chondrogenic self-organisation of embryonic limb bud cells in micromass culture.

Draft Manuscript: Pattern formation in micromass culture

Rebecca A Rolfe*[1], Claire Shea*[1] and Paula Murphy[1]

[1]Department of Zoology, School of Natural Sciences, Trinity College Dublin, The University of Dublin, Ireland

*Authors contributed equally to the work

Correspondence: Department of Zoology, School of Natural Sciences, Trinity College Dublin, Dublin 2, Ireland.
Phone: +353 1 896-3580
Email: paula.murphy@tcd.ie

Draft for re-submission following first review to
Cell and Tissue Research

Keywords: Chondrogenesis, micromass culture, self-organisation, pattern formation, ArcGIS

Abstract

Spatial and temporal control of chondrogenesis generates precise, species-specific patterns of skeletal structures in the developing vertebrate limb. The pattern-template is laid down when mesenchymal cells at the core of the early limb-bud condense and undergo chondrogenic differentiation. Although the mechanisms involved in organising such complex patterns are not fully understood, the interplay between BMP and Wnt signaling pathways is fundamental. Primary embryonic limb bud cells grown under high-density micromass culture conditions spontaneously create a simple cartilage nodule pattern, presenting a model to investigate pattern generation. We describe a novel analytical approach to quantify geometric properties and spatial relationships between chondrogenic condensations, utilizing the micromass model. We follow the emergence of pattern in live cultures with nodules forming at regular distances, growing and changing shape over time. Gene expression profiling supports rapid chondrogenesis and transition to hypertrophy, mimicking the process of endochondral ossification within the limb bud. Manipulating the signaling environment through addition of BMP or Wnt ligands, as well as the BMP pathway antagonist Noggin, altered the differentiation profile and nodule pattern. BMP2 addition increased chondrogenesis while WNT3A or Noggin had the opposite effect, but with distinct pattern outcomes. Titrating these pro- and anti-chondrogenic factors and examining the resulting patterns, supports the hypothesis that regularly spaced cartilage nodules formed by primary limb-bud cells in micromass culture is influenced by the balance of Wnt and BMP signaling under a Turing-like mechanism. This study demonstrates an approach for investigating the mechanisms governing chondrogenic spatial organization using simple micromass culture.

Introduction

Micromass culture is a well-established approach for assaying chondrogenic potential, where cells are plated in a simple high-density, microdrop culture, that can induce cellular aggregation and chondrogenic differentiation, mimicking the process of mesenchymal condensation during skeletogenesis (reviewed in Bobick et al., 2009). A major advantage of this system is its simplicity, where chondrogenesis can be monitored temporally. It is a highly adaptable model that allows for testing of a variety of conditions including the application of soluble factors (Bobick et al., 2014; Francis-West et al., 1999; Mello and Tuan, 2006) and the effects of mechanical stimulation (Juhasz et al., 2014; Klumpers et al., 2015; Saha et al., 2017). A striking aspect of micromass cultures made from primary embryonic limb bud cells is the generation of a self-organised spatial pattern of chondrogenic nodules (Butterfield et al., 2017; Christley et al., 2007; Mello and Tuan, 1999; Raspopovic et al., 2014; Saha et al., 2017). This innate property is also demonstrated in the embryonically-derived cell line ATDC5 (derived from mouse embryonic teratocarcinoma) (Seemann et al., 2005); however, the cell line C3H10T12 (derived from mouse embryonic sarcoma) fails to form distinct nodules, yet expresses chondrogenic marker genes (Takacs et al., 2013). Thus, the capacity to spontaneously form regular, spatially-organised patterns of cartilage nodules is preserved in one of the embryonically derived cell lines and not the other. Although little is known about the mechanisms that underpin this self-assembly process, the micromass culture system provides a convenient opportunity for further investigation.

In the developing limb, spatial and temporal control of chondrogenesis and condensation of chondrogenic cells generates precise, species-specific patterns of limb skeletal structures. The majority of cells within mesenchymal cell condensations at the core of the developing limb bud differentiate into transient cartilage (marked by activation of *Sox9* and *Col2a1* genes), later undergoing hypertrophy (marked by activation of *Ihh* and *Col10a1* genes), followed by ossification to form the early bones (reviewed in Long and Ornitz, 2013). Cells at the joint interface however do not progress to hypertrophy but rather form the stable, permanent, articular cartilage of the future joint. The precise molecular mechanisms and physical cues that define these distinct, spatially appropriate differentiation programs, have not been fully elucidated. Recent work examining the effect of biophysical stimulation has shown that canonical Wnt signaling and BMP signaling are two major pathways involved in the distinctive differentiation of these two cartilage types within the rudiment (Ray et al., 2015; Rolfe et al., 2018; Singh et al., 2018).

It is well-recognised that morphogen gradients are responsible for establishing proximo-distal and antero-posterior axes in the limb bud, and models incorporating Turing reaction-diffusion mechanisms have been proposed to explain the robust formation of skeletal elements in the limb skeleton (reviewed in Delgado and Torres, 2016; Glimm et al., 2020). Specifically, the interaction of BMP and Wnt signals has been proposed to regulate Sox9 expression and the formation of regularly-spaced digits within the digital plate in a Turing-like reaction-diffusion mechanism (Raspopovic et al., 2014). In this model, BMP and canonical Wnt signaling act as pro- and anti-chondrogenic factors to generate characteristic patterns within the digital plate, proposed to be reflected in the pattern generated in micromass cultures. This study further showed that both Sox9-positive (pre-cartilage) and -negative (non-cartilage) cells derived from embryonic limb buds are capable of establishing nodule patterns in micromass culture, demonstrating that the formation of cellular condensations is not based on pre-determined cell fate but on whole-culture dynamics, which could be influenced by concentration/diffusion of signaling molecules and mechanical characteristics within the culture.

A robust method to quantitatively describe and assess condensation formation in micromass culture would therefore provide a means of examining proposed mechanisms that underlie pattern generation *in vitro*, allowing more comprehensive comparison of the patterns formed under different conditions. Some studies have employed sophisticated modelling approaches to investigate chondrogenic pattern formation in micromass culture (Christley et al., 2007; Miura and Shiota, 2000a, b), others have measured periodicity and the shape and size of individual nodules (Butterfield et al., 2017; Duke et al., 1998) and more recently inter-condensation distances (Bhat et al., 2019). In this study, we develop novel methods to systematically quantify the spatial pattern of chondrogenic condensations that form from embryonic limb bud-derived cells in an experimental setting. We examine the self-organising pattern as it emerges and changes over time and how it responds to changes in the signaling environment by addition of soluble factors. We demonstrate that modulation by treatment with BMP2 or WNT3A recombinant proteins results in opposing effects on the self-organisation pattern, with BMP resulting in more nodules that are closer together, while WNT3A reduces condensation formation. Furthermore, we demonstrate that titration of these pro- and anti-chondrogenic signaling molecules adjusts the balance of condensation formation. This study expands our knowledge on the balance of signaling molecules involved and also presents an experimental method for quantifying biological spatial patterns *in vitro.*

Materials and Methods

Embryonic limb micromass cell culture

CD1 mice housed in the Bioresources Unit Trinity College Dublin were mated over-night. The morning of detection of vaginal plugs was designated as Embryonic day (E) 0.5 with collection of embryos on E10.5, E11.5 and E12.5 according to the regulations of the HPRA (Health Products Regulatory Authority), Ireland, by a licensed individual. Micromass cultures were set up as detailed in Saha et al. (2017), with minor adjustments. Micromass drops (15 µl) were plated at a density of 1-2 x10^7 cells per ml either directly on tissue-culture grade treated plastic dishes (Thermo Fisher/Nunc 176740 or 142485), or on 10 mm glass coverslips (Invitrogen 12658116) pre-treated with 0.015M poly-D-ornithine (Sigma). Drop cultures adhered in an incubator (37°C and 5% CO_2) before being flooding with 400 µl of growth medium (Dulbecco's F-12 Ham's medium [DMEM/F12] [Sigma] plus 2 mM L-Glutamine [Life Technologies], 100 units/ml Penicillin/Streptomycin [Life Technologies], 50 µg/ml Ascorbic acid [Sigma] and 10% Fetal bovine serum [FBS; Sigma]) alone or supplemented with either human WNT3A (R&D Systems 5036-WN), human BMP2 (R&D Systems 355-BM) or human Noggin (R&D Systems 719-NG) for final concentrations between 10-200ng/ml. The medium was changed on alternate days by removing half the well volume and replacing it with an equal volume of fresh medium. Cultures were harvested every 12 hours or every 48hrs until 144hrs.

Alcian Blue staining

Micromass cultures were washed in Phosphate Buffered Saline (PBS), fixed in 4% Paraformaldehyde (PFA) in PBS for 30 mins, rinsed twice in PBS and stained with 1% Alcian Blue (8GX, Sigma A5268) in 0.1 M HCL for 30 mins at room temperature. Cultures were washed and mounted on glass slides or stored in PBS. Slides were photographed using an Olympus SZX12 microscope; images of whole micromass cultures were taken on an Olympus dissecting microscope.

Image analysis and nodule geometries

Images of Alcian Blue-stained micromass cultures were processed using ImageJ (Version 1.51j8; National Institutes of Health, USA). Original files (Fig 1a) were cropped to define the region of interest (ROI) to a circle of 5 mm diameter which was centred over the micromass (Fig 1b). Images were 'cleaned' by encircling debris/ artefacts (not nodules) with the Freehand tool and filling the enclosed space with white (Fig 1c, red arrow). Cleaned images were split into component colour 'channels' (Fig 1d-d''), the green channel was determined to have the best signal-to-noise ratio and so was used for further analysis (Fig 1d'). Images were converted

to an 8-bit black and white image by setting a minimum threshold, using the auto-threshold function as a guideline. This converted every pixel above the threshold in the greyscale green channel image to black, and every pixel below the threshold to white (Fig 1e). Treatment groups within an experiment had the same threshold value applied, but the appropriate threshold values were determined independently for each experiment, due to unavoidable variability in staining contrast or intensity, and in image capture. Any background noise was removed (Fig 1e, red arrowhead) and converged nodules were separated using the Despeckle and Watershed functions (Fig 1f, green arrowhead). At this stage, images were further cropped to a circular ROI with a 2-mm diameter, centred within the larger 5 mm region of interest. Both the 5 mm and 2 mm images were used for analysis.

Nodules were counted and measured using the Analyse Particles function (Fig 1g), with a minimum particle size of 0.005 μm^2. The total nodule count was done using the 5-mm ROI. Manual counts of nodule number were compared to automated counts, to ensure accuracy of the method; no difference was found between manual and automated counts (data not shown). Other parameters, including the size of each detected nodule (in μm^2), the area covered by nodules (%) and shape descriptors such as circularity and solidity were based on the 2-mm ROI. Nodules touching the edge of the circular frame were excluded to prevent inaccurate size measurements. Exclusion of nodules at the edges could affect the measurements of nodule spacing and proximity slightly, but this was tested, and the difference was determined not to be significant. Automation of the procedure was performed by establishing command macros within ImageJ (Supplemental material 1). At earlier time points (i.e. <48hrs), cell condensations are very faint in appearance, even after Alcian Blue staining, and automated processing ensures that nodules are counted accurately by setting a threshold level. Automated watershedding, as described above, separates detected objects which overlap. When counting manually, these individual nodules were sometimes not easily distinguishable, especially at later time points (e.g. 144hrs), when nodules had grown and their edges appeared merged. Therefore, watershedding effectively separated nodules in an unbiased manner.

The Analyse Particles function generated shape measures of circularity and solidity for each detected nodule. Circularity is the measure of how close to a perfect circle a given shape is, as calculated by 4π times the shape area divided by the shape perimeter squared. A perfect circle has a circularity value of 1.0; as the shape becomes more elongated (ellipsoid), its circularity value decreases (Fig 1h). Solidity is an indicator of the convexity, or "smoothness", of an object, as calculated by shape area divided by the convex hull area (Fig 1i). The convex area is the area of the smallest ellipse that can be drawn around the object, completely enclosing it. A

circle or ellipse has a solidity value of 1.0; if the shape has more concave features (is "rougher"), the solidity value decreases.

To quantify nodule to nodule spatial relationships, the spacing and proximity of nodules were calculated (Fig 1j-k). To measure spacing, the distance between a given nodule's centre point and the nearest centre point of another nodule was calculated for each nodule in each micromass (Fig 1j, red dots). ImageJ Analyse Particles function generated x and y co-ordinates of the centre point of each detected nodule, which were analysed using the spatial point pattern analysis package "Spatstat" in RStudio (v.1.1.463) (Fig 1g), To measure proximity a method was devised, based on Geographical Information Systems (GIS) analysis, where the distance between a point on the perimeter of a given nodule and the closest point on the perimeter of a distinct neighbouring nodule was calculated (Fig 1k, green dots) using ArcGIS software and Python programming (v.3.7.2) (Fig 1k). Details of the script used for nodule spacing (nearest neighbour distances - centre-points) and nodule proximity (nearest neighbour distances – edges) are specified in detail in supplementary material 2.

A minimum of 3 biological replicates were analysed in 3 independent experiments for cultures up to and including 48 hrs, and a minimum of 5 independent biological replicates in independent experiments for 48 hrs, 96 hrs and 144 hr cultures. Each experiment consisted of 2-6 replicates in each group, that were processed for Alcian Blue staining and pattern analysis. SPSS statistics (IBM®, v.26) was used for statistical analysis. In order to assess significance over time and between groups at each timepoint, one-way ANOVA was performed, followed by Tukey's post hoc test with a 95% confidence interval. P values of ≤ 0.05 were considered significant.

RNA extraction, cDNA synthesis, and real time quantitative gene expression analysis by Reverse Transcription-Polymerase Chain Reaction (RT-PCR)

For RNA extraction, individual micromass cultures were treated with 100µl TRIzol reagent for 2 mins. Following mechanical homogenisation of the cell-Trizol solution with a pipette tip, multiple micromass cultures (2-4 per growth condition) were pooled to increase RNA quantity for analysis. Day 0 control RNA was obtained from 10-30 µl of cell suspension added to TRIzol on the day of cell harvest. All samples were stored at -80°C until further processing. RNA was extracted with chloroform and purified with a TRIzol Purelink kit (Invitrogen) or an RNA miniprep kit (Qiagen) following manufacturers' instructions. Typically, RNA was re-suspended in 30 µl of nuclease-free water and quantified using the Qubit 2.0 Quantitation System (Invitrogen).

Primers were designed using Primer Express Software®, version 3.0 under default settings for TaqMan® quantification and purchased through Sigma (Sigma-Aldrich, Ireland), as listed in Table 1; *Gapdh* was used as the normaliser transcript. mRNA was reverse transcribed using a standard quantity of total RNA (100 ng) and High Capacity cDNA Reverse Transcription Kit (Applied Biosystems™: 4368814), diluted 1:5 with RNase free water. Real-time PCR quantification was performed using an ABI 7500 as described in Saha et al. (2017). Three technical replicates were processed within each qPCR assay. A minimum of 3 independent experimental replicates for all cultures up to and including 48 hrs, and a minimum of 5 independent experimental replicates for Growth medium conditions and 2-5 independent experimental replicates for Bmp2 and WNT3A protein addition for 48 hr, 96 hr and 144 hr cultures were combined for analysis.

Results

Chondrogenesis and establishment of an organised pattern of cell condensations occurs rapidly in micromass cultures

Primary limb bud cells obtained from E11.5 embryos grown in high density micromass cultures in Growth Medium (GM), show the first appearance of visible cell condensations by 24 hours (hrs) (Fig 2a). Tracking these condensations over time confirmed that they correspond to the site of future chondrogenic nodules, first clearly identifiable through Alcian Blue staining by 48 hrs, becoming more distinct at 96 and 144 hrs (Fig 2a & b). Molecular profiling of chondrogenesis using qRT-PCR to monitor expression of marker genes confirmed early chondrogenic differentiation (Supplementary Fig 1), in line with previous studies (Saha et al., 2017). The chondrogenic marker Col2a1 was significantly upregulated by 96 hrs (14.7 ± 4.4 fold; 26.5 ± 7 Fold at 144 hrs), with an earlier increasing trend in mean expression values from 36 hrs (compared to E11.5 limb bud cells at time 0 [prepared for plating]). Expression of Col10a1, a marker of hypertrophy, increased significantly at 144 hrs (15.5 ± 7.5 fold, $p=0.034$). These data represent 5-6 independent experiments with high levels of variation between experiments, particularly at 144 hrs. Although mean expression of Sox9 (early chondrogenic marker) and Ihh (pre-hypertrophic marker) increased over time, in the context of the large variation between experiments, neither reached significance at the 95% confidence level. Elevation of the mean expression level of Ihh, at 36 hrs (8.1 ± 1.6 fold, $p=0.07$) aligns with previously reported data for a transient up-regulation already at day 1 of culture (Saha et al.,

2017), and overall the trends align with rapid chondrogenic differentiation and progression to hypertrophy (Supplementary Fig. 1).

The visible pattern of chondrogenesis was considerably different with cells obtained from earlier (E10.5) or later (E12.5) limbs buds (Supplementary Fig 2), corresponding to previous reports in the chick limb (Ahrens et al., 1977): Using E10.5 limb bud cells, nodules were significantly larger, while nodules were significantly smaller from E12.5 limb bud cells. While there was a higher average number of nodules formed from E11.5 limb buds, this was variable and not significant (Supplementary Fig 2).

In order to describe the pattern of chondrogenic nodules in a systematic and quantitative way, we developed an automated, high-throughput process to capture features of the pattern: number of nodules, nodule size, area covered by nodules, circularity, solidity, spacing between nodule centres and proximity of nodule edges (Fig 1; Fig 2c-i). The number of nodules increased dramatically from 48 hrs to 96 hrs (6 ± 1 [48 hrs] to 240.9 ± 19.4 [96 hrs], $p \leq 0.001$), with no further increase to 144 hrs (Fig 2c). The average % area covered by nodules (in a 2mm ROI) significantly increased at 96 hrs, further increasing by 144 hrs (12.5 ± 1.9% and 20.2 ± 1.4%, respectively $p \leq 0.001$; Fig 2d). This increase in area coverage corresponds to increase in nodule size, particularly between 96 hrs and 144 hrs (Fig 2d, e). These descriptors reflect observed nodule formation (Fig 2a, b) with no new nodules forming but nodules expanding in size between 96 hrs and 144 hrs. Note that as adjacent nodules increase in size some form continuous lines of Alcian Blue staining (Fig 2a'').

Individual nodule shape was analysed to monitor the characteristics of nodule growth using circularity and solidity parameters. Circularity is a measure of how close to a perfect circle a given shape is (value of 1.0); the lower the value, the less circular the shape. The average nodule circularity score decreased from 48 hrs (0.98 ± 0.01) to 96 hrs (0.82 ±0.01) with nodules becoming less circular as they mature and enlarge (Fig 2g). Solidity is an indicator of how smooth the outline is with lower values reflecting a "rougher" shape. Nodules became "rougher" during the period of nodule formation (between 2 and 4 days) but once all nodules are formed, they become smoother (between 96 and 144 hrs) (Fig 2h).

For nodule-to-nodule relationships, while there is a dramatic drop in distances between 48 hrs and later timepoints, between 96 and 144 hrs there is no change in the distance between nodule centres (which corresponds to no new nodules being formed) and a decreasing trend in distance between nodule edges (although not significant, this reflets the increase in nodule size). Strikingly, the large variance in distance measurements at 48 hrs reduces at later time points

indicating that the pattern becomes more regular as it establishes, with constant distance between nodule centre points and edges.

Manipulation of the signaling environment alters the pattern of chondrogenesis with BMP and Wnt signaling pathways acting as pro and anti-chondrogenic factors.

We investigated the effect of altering the BMP and Wnt signaling environment on the establishment of the self-organised pattern of chondrogenic nodules in micromass cultures compared to growth medium. Upon addition of 100ng/ml BMP2 (bone morphogenetic protein 2) protein, clearly identifiable Alcian Blue-positive chondrogenic nodules were observed by 48 hrs, similar to GM conditions (Fig 3a,b). Treatment with 200ng/ml WNT3A protein resulted in a dramatic reduction in the formation of Alcian Blue-positive nodules across the entire timeframe examined (Fig 3c), with replicate experiments showing no or very few stained nodules at 96 and 144 hrs (Supplementary Fig 3).

Geometric analysis of the nodule pattern showed an increase in the average number of nodules over time with added BMP2, with a temporal profile similar to GM conditions, but with an increase in the number of nodules formed under BMP2 treatment at 144 hrs (310.3 ± 23.5) compared to GM alone (220 ± 20.1, $p \leq 0.01$) (Fig 3d). There was also a significant increase in the area covered by nodules (Fig 3f), while the average size of nodules at 144 hrs did not increase (Fig 3e). The distance between nodule centre points and nodule edges was significantly reduced at 144 hrs with BMP2 treatment compared to GM (Fig 3h, i). Thus, at 144 hrs, BMP2 treatment resulted in a larger number of distinct nodules, spaced closer together, which therefore cover a larger area, but are not individually larger in size.

Contrastingly, with WNT3A addition there was a reduction in the number of nodules, nodule size and therefore area coverage (Fig 3d, e, f). The shape of the WNT3A treated nodules present at 96 hrs and 144 hrs were more circular than those in the GM or BMP2 groups (Fig 3g). A striking effect of WNT3A addition was the irregular spacing of the few nodules that formed (Supplementary Fig 3 represents the variability seen at 144 hrs with 200ng/ml WNT3A treatment across six experiments); therefore, due to enormous variation in the patterns produced in the +WNT3A cultures, inter-nodule relationship data are presented for GM and +BMP2 cultures only. (The variation in nodule spacing seen on the addition of WNT3A is explored further in the next section). Taken together, these data reveal that while addition of BMP2 increases nodule formation over 144 hrs, resulting in more nodules with centres and edges closer together, activation of canonical Wnt signalling significantly reduces the appearance of nodules and the pattern is more irregular. Analysis of these geometric descriptors

demonstrates that introduction of signalling molecules alters the chondrogeneic profile and pattern of cartilage condensations, with BMP and canonical-Wnt signalling acting as pro and anti-chondrogenic factors.

qRT-PCR analysis showed that addition of BMP2 results in a profile of chondrogenic and hypertrophic marker expression over time similar to GM, for example, increase in expression of Col2a1 reaching significance at 96 hrs (14.9 ± 5.9 fold, p=0.002) and 144 hrs (15.1 ± 4.1 fold, p=0.001) (Fig 3j; Supplementary Fig 4). Sox9 expression levels showed a significant increase at 48 hrs (2.6 ± 0.4 fold, p=0.02), whereas GM produced a more steady increasing trend over time (Supplementary Fig 4). Higher overall expression levels were observed for the pre-hypertrophic chondrocyte marker Ihh, in the presence of BMP2 with a significant increase compared to time 0 at 36 hrs (22.1 ± 5.2 fold, p=0.04; Supplementary Fig 4) and significant increase compared to GM at 24 hrs (20.1 ± 7 fold, p=0.018; Fig 3k). Expression of the hypertrophic maturation marker Col10a1 also demonstrated a similar profile to GM with increase over time, although with consistently higher mean levels (e.g., at 36 hrs 13.4 ± 5.4 fold compared to 8.19 ± 5.9 fold; at 48 hrs, 11.2 ± 3.6 fold compared to 4.5 ± 2) (Supplementary Fig 4) consistent with increased Ihh expression and an earlier shift toward a hypertrophic chondrogenic phenotype.

With addition of WNT3A the gene expression profile supports the nodule pattern analysis with consistently low levels of chondrogenic markers Sox9 and Col2a1; Col2a1 is already significantly downregulated at 12hrs compared to time 0 (Fig 3j and Supplementary Fig 4) and both Col2a1 and Sox9 are downregulated compared to GM and/or BMP2 conditions across the time profile. Markers of hypertrophic maturation (Ihh and Col10a1) in the presence of WNT3A show large variability across experiments (n=3)-and, surprisingly, show transient up-regulation at 12 hrs (Ihh; Fig 3k) and 24 hrs (Col10a1; Supplementary Fig 4) compared to time 0. There were no significant differences compared to GM conditions for markers of hypertrophy, although the large variability should be noted.

These results, taken together, suggest that the qualitative and quantitative profile of chondrogenesis in GM, with rapid chondrogenic differentiation once cells are plated in high density micromass cultures, is enhanced with addition of BMP signaling ligand. In contrast, activation of Wnt signaling prevents chondrogenic differentiation.

Titration of the effects of BMP and Wnt: Adjustment of the equilibrium of signaling molecules alters the chondrogenic pattern in micromass culture.

In order to further investigate the opposing effects of BMP and Wnt on the chondrogenic pattern in micromass culture, we titrated the concentration of added BMP2 and WNT3A proteins, examining the resulting pattern of nodules after 144 hrs. For comparison, to further explore the mechanism, we additionally investigated the effect of adding the BMP pathway antagonist, Noggin (NOG). Fig 4a shows nodules formed as a proportion of the number of nodules formed in GM when the concentration of each additive is varied between 50-200ng/ml for WNT3A, 10-200ng/ml for Noggin and 10-100ng/ml for BMP2. Fig 4b-d shows the data for nodule size, area, spacing and proximity. Supplementary Table 1 shows the direction of change and level of significance for all parameters and comparison of all treatments with GM (Supplementary Table 1a), as well as intertreatment comparisons (Supplementary Table 1b). It is clear that as the concentration of added BMP2 increases the number of nodules increases, the size of individual nodules does not, while the spacing between nodules decreases. With addition of the lowest concentration of BMP2 (10ng/ml), there is already a significant increase in nodule number and significant decrease in spacing. The dose effect is not linear.

The addition of WNT3A and Noggin both lead to progressively fewer nodules, reduced nodule size and increase in the spacing between nodules as increasing amounts of protein are added. Addition of the lowest doses of WNT3A (50ng/ml) and Noggin (10ng/ml) had little effect on any parameter while further increasing dosage of either showed reductions in nodule number and size and increase in spacing.

To get an overview comparison of the effects, Fig 4e shows trend traces for the average values for several parameters across dosages. The opposing effects of both WNT3A and NOG compared to BMP2 are striking across parameters. Comparing WNT3A and NOG effects however we see that while they both reduce chondrogenesis, the effects are distinct. Decreases in nodule number, size and coverage are closer to linear for NOG than WNT3A (Fig 4e), for example as the NOG concentration was reduced there was a linear reduction in the extent of the difference in number, size and area coverage, with the intermediate concentration (50ng/ml) still showing significant differences to GM (Fig 4b-d, Supplementary Table 1a). While circularity increases with both additives, the effect is more dramatic with WNT3A. More strikingly, while both factors lead to increase in the spacing, the regular spacing between nodules that is characteristic of micromass patterns is ~~more~~ dramatically lost with the addition of WNT3A; this is reflected in the very large variance in spacing and proximity measurements upon addition of 100ng and 200ng/ml WNT3A (Fig 4c; Supplementary Fig 5), where regular spacing is lost. To further demonstrate the increased variability in nodule spacing across individual micromass cultures upon addition of WNT3A, Supplementary Fig 5 shows analysis

of individual replicates across experiments, compared to GM. Note that there is increased variability even at the lowest concentration of 50ng/ml even though this level of WNT3A treatment does not significantly reduce the number of nodules formed (Fig 4a). This indicates a difference in the mechanisms of interference with the pattern of chondrogenesis when BMP signaling is blocked (NOG) and canonical Wnt signaling is activated.

Discussion:

Micromass culture is a valuable tool for a variety of studies; from assaying chondrogenic potential and examining the effect of changing the molecular or mechanical environment on chondrogenic differentiation, to computational modelling of the pattern of nodules that form spontaneously within the culture (Bobick et al., 2014; Christley et al., 2007; Francis-West et al., 1999; Klumpers et al., 2015; Miura et al., 2000; Norrie et al., 2014; Raspopovic et al., 2014; Saha et al., 2017). The regular pattern of chondrogenic nodules that typically forms when primary embryonic limb bud cells are placed under micromass culture conditions is the result of whole culture dynamics (rather than pre-determination), where the foci of differentiating cells self-organise within the culture environment (Raspopovic et al., 2014) and where a Turing like reaction-diffusion mechanism has been proposed to underlie pattern generation (for example Christley et al., 2007). Chondrogenesis in micromass culture has been measured quantitatively using qRT-PCR analysis of marker genes, with rapid increase in both chondrogenic markers (e.g. Sox9 and Col2a1) and markers of hypertrophy (e.g. Ihh and Col10a1)(Saha et al., 2017), while the pattern of nodule formation is often described more qualitatively with limited use of quantitation. Here we present a novel approach that systematically captures characteristic aspects of the emerging patterns quantitatively. We use the analysis to profile the generation of discrete chondrogenic nodules over time. We show rapid formation of cellular condensations by 24 hrs in culture and, by tracing the elaboration of the pattern in live cultures, that these condensations become the Alcian Blue positive cartilage nodules detectable by 48 hrs. We show that nodules form at regular distances from each other, grow in size becoming elongated and rougher, with the edges of adjacent nodules coming closer together over time. In parallel, monitoring the expression of marker genes showed profiles consistent with previous studies (Saha et al., 2017), while we noted high levels of variation between experiments. We further analysed the effect of changing the signaling environment on the pattern, with addition of pro-chondrogenic (BMP2) and anti-chondrogenic (WNT3A and NOG) factors. By titrating the concentration of added factors and comparing the effect of Wnt to the BMP antagonist Noggin, we demonstrate how pattern analysis can be used

to explore the mechanism(s) involved in pattern generation. We show that although Wnt and Noggin addition both decrease chondrogenesis and nodule number, the effects on the pattern are distinct, indicating that they affect the signaling balance in different ways.

The ability of limb bud cells to spontaneously differentiate, forming regularly spaced nodules reflects an intrinsic capacity to self-organise into this relatively simple pattern and allows for the examination of the basis of such pattern generation. Analysis of the spatial pattern quantitatively is therefore of particular value. The methodology developed here was inspired by large-scale ecological data analysis that quantifies and classifies geographical areas and compares the spacing and proximity of specific parameters using Geographical Information Systems (GIS). We adapted ArcGIS software that is commonly used as a tool to identify spatio-temporal patterns, including viral infections, disease outbreaks and spread (Cunze et al., 2018; Nyakarahuka et al., 2017; Olanrewaju and Adepoju, 2017), the ecological stability of plant species (Miao et al., 2016) and analysis of vacant land for reuse (Newman et al., 2017). In applying this methodology, we treated images of whole cultures (landscapes) as 'maps' and nodules as 'islands' to analyse the spatial relationships amongst them. Previous quantitative analysis of micromass cultures have counted nodules (Bhat et al., 2019; Duke et al., 1998; Saha et al., 2017), measured total chondrogenic area and nodule size (Butterfield et al., 2017), and distances between nodules by utilising binary image processing to quantify periodicity in chondrogenic patterns (Christley et al., 2007; Mello and Tuan, 1999; Miura et al., 2000). Similarly, we use binarisation of images to segregate chondrogenic and non-chondrogenic areas, however in contrast to our approach, previous studies utilised a skeletonisation function to identify the centre line of each chondrogenic area (described in Miura et al., 2000). Thus, while focusing on the average interval between nodules~~,~~ parameters such as nodule size, shape, and nodule to nodule edge distances were not integrated. A benefit of our approach using ArcGIS, is that it examines multiple parameters including both nodule centres and edges and thus allows a richer examination of the relationship between nodules. For example, it revealed that while addition of increasing concentrations of BMP2 leads to nodules with centre points progressively closer together (Fig 4c), the proximity of nodule edges only significantly changed at the highest level of BMP2 treatment (Fig 4d). The benefit of this approach therefore is that it captures greater detail in monitoring patterns over time and under different treatments; it enables an experimental approach to quantify biological spatial patterns generated in simple culture, results from which can be used in computational models to investigate more specific hypotheses regarding self-organisation and pattern formation *in vivo*.

The effects of BMP and Wnt signaling are of prime interest for this study because of their

importance in the spatially appropriate control of cartilage differentiation at forming joints and digit patterning (Raspopovic et al., 2014). In a model proposed by Ray et al. (Ray et al., 2015), adjacent territories of BMP and Wnt signaling underlie the spatial distinction between transient cartilage that acts as a template for bone formation and stable cartilage formation at the joint. We have previously shown that when mechanical stimulation from movement is reduced in both chick and mouse models, the BMP active territory within the skeletal rudiment expands across the joint zone, accompanied by joint line reduction and rudiment fusions (Rolfe et al., 2018; Singh et al., 2018). It is well established that BMP signaling enhances chondrogenesis in culture (Brady et al., 2014; Carlberg et al., 2001; Mendes et al., 2016; Saha et al., 2017) and, *in vivo*, overexpression of Bmp2 in the embryonic limb has been shown to induce formation of cartilage at the expense of articular cartilage (Duprez et al., 1996). The findings in the present study of increased chondrogenesis upon addition of BMP2 is therefore of no surprise. The importance of BMP signaling for nodule formation within the culture is further reinforced by the anti-chondrogenic effect of addition of the BMP antagonist Noggin. Although the influence of Wnt signaling on skeletogenesis is challenging to unravel, with the potential involvement of multiple Wnt ligands, Frizzled receptors and pathway modulators (Summerhurst et al., 2008), it has been shown that Wnt signaling activity is suppressed during initial chondrogenic differentiation, but is simultaneously active at the joint interzone, where cartilage formation is inhibited (Day et al., 2005; Guo et al., 2004; Rolfe et al., 2018; Singh et al., 2018; Spater et al., 2006). Also, embryonic misexpression of canonical Wnt pathway ligands or overexpression of β-catenin has been shown to accelerate chondrocyte hypertrophy, induce gaps in cartilaginous rudiments and upregulate joint specific genes, suggestive of the formation of ectopic joints (Hartmann and Tabin, 2000, 2001; Rolfe et al., 2018). This is aligned with the finding here that addition of the canonical Wnt ligand, WNT3A resulted in an overall reduction in expression of chondrogenic genes and a widespread reduction of chondrogenic nodules. Rudnicki and Brown (1997) also previously showed that expression of Wnt1 or Wnt7a using retroviral infection abolished nodule formation (Rudnicki and Brown, 1997). The more surprising and illuminating finding here is that addition of WNT3A not only reduced the number of nodules but also abolished regular distancing between nodules.

A Turing mechanism involving interplay between BMP and Wnt signaling and Sox9 expression has been proposed to regulate the repeated pattern of digit formation in the distal limb bud (Raspopovic et al., 2014). A key feature of Turing mechanisms is their ability to self-regulate or modulate output patterns based on integration of signals (reviewed in Kondo and Miura, 2010). The regular spacing of nodule formation events in micromass cultures recalls

the spacing of digits in developing hand and footplates, and, is also speculated to be the result of such a Turing mechanism, with different parameters (Christley et al., 2007; Miura et al., 2000; Miura and Shiota, 2000a; Raspopovic et al., 2014). The alteration and titration of the signaling environment in this study indicates that adjusting the signaling balance systemically can impact the regular spacing of nodule formation which could be a result of adjusting the parameters in such a Turing mechanism. A robust method to quantitatively describe and assess nodule formation in micromass culture, as presented here, therefore represents a way to inform testing of proposed Turing mechanisms *in vitro*, to elucidate the parameters involved in the phenomenal ability of these cells to self organise spatially. While it is unclear whether the mechanisms underpinning the periodic patterns in micromass culture and in digit formation *in vivo* are the same, our experimental results provide supportive evidence for relationships between the patterns.

Titration of the concentration of added factors to the cultures was valuable in revealing more detail of the effects on the chondrogenic pattern. In all cases, as the concentration of added BMP2, WNT3A and NOG was reduced, the patterns became more similar to that observed in Growth Medium (GM) (Fig 4a), however the effect of increasing concentration of NOG was linear, whereas for BMP2 and WNT3A, lower augmentation levels had proportionally less effect on the pattern. Since Noggin is known to bind BMPs with high affinity (especially 2, 4 and 7) (reviewed in Krause et al., 2011; Zimmerman et al., 1996), this response aligns with a mechanism of sequestration of active BMP under GM culture conditions. It is notable that while increase in the concentration of BMP2 and NOG in the culture media had clear pro- and anti-chondrogenic effects, a pattern of nodules still emerges, showing that changing the systemic concentration within these ranges does not abolish the ability to generate a self-organised pattern. Under the proposed Turning mechanism, this suggests that it does prevent the establishment of reaction-diffusion dynamics. By contrast WNT3A systemic augmentation at 100ng and 200ng/ml abolishes the regular pattern as well as suppressing chondrogenesis. It is interesting to note that previous modelling predicted that if exposure to the activator (BMP in this scenario) is too short, the nodule size would be reduced and the pattern irregular (Christley et al., 2007). The distinct profile of effects of the two anti-chondrogenic factors, WNT3A and NOG, favours a more indirect interplay between Wnt and BMP with increase in the Wnt concentration disrupting the spatial pattern rather than reducing the frequency of differentiation foci (Fig 4c, d, e). Indirect interaction Between Wnt and BMP signaling is a feature of the reaction-diffusion model proposed by Raspopovic et al (Marcon et al., 2016; Raspopovic et al., 2014).

It is interesting to compare the micromass pattern produced by limb bud cells derived at different developmental time points grown in GM (Supplementary Fig 2) to the effects of signaling molecule addition at E11.5. While addition of BMP2 led to larger nodules covering more area, reminiscent of cultures prepared from the earlier stage, E10.5 limb buds, addition of NOG and WNT3A led to formation of smaller nodules covering less area, reminiscent of cultures produced at the later timepoint of E12.5 (Supplementary Table 1 a; Supplementary Fig 2). It would be interesting to investigate the level of BMP and Wnt signaling active within the limb bud across E10.5- E12.5. One indirect means of assessing the level of canonical Wnt signaling would be measuring the activity of read-out genes within the limb buds of canonical Wnt reporter mice (for example: Ferrer-Vaquer et al., 2010; Maretto et al., 2003).

While the micromass culture system has to date been valuable in assessing chondrogenesis, this study reveals greater potential for further insight if the pattern of chondrogenic output is analysed more comprehensively. Chondrogenic output is often measured by quantitative assessment of marker gene expression and while the use of qRT-PCR in this respect is valuable, we found high levels of variation between independent micromass experiments (Supplementary Fig 1 and (Saha et al., 2017)). The marker gene expression profile revealed here was in line with previous studies and reflected the chondorogenic output revealed by analysis of the pattern of nodules formed, however nodule pattern analysis gave a more consistent quantitative measure. Micromass assays can be used to assess a wide range of soluble and physical cues, enabling well-controlled investigation of the role of these varied cues in guiding tissue patterning and boundary formation in skeletal development. For example, the adjustment of substrate stiffness or other aspects of the physical environment, of oxygen tension (recapitulation of embryonic levels), or cytoskeletal mechanics, as well as further exploration of signaling molecules. The effect of creating local gradients of signaling molecules would be of particular interest especially in light of the debate about the relative importance of spatially graded molecular cues and self-organising mechanisms, and the interplay between them (Green and Sharpe, 2015). To date micromass culture has been used to investigate cellular response to the mechanical environment (Juhasz et al., 2014; Onodera et al., 2005; Saha et al., 2017), but combining this with manipulation of the signaling environment holds great potential for furthering our understand of how skeletal patterning is established and tissues organised with wide significance to the fields of synthetic biology and regenerative medicine.

Conclusion:

This study provides a description of the geometric self-organisation of chondrogenic

condensations formed from embryonic limb bud cells in micromass culture. It utilises a novel geographical approach in the examination of whole culture patterns of chondrogenesis over time and the impact of molecular manipulation on chondrogenic pattern formation. This analysis captures more quantitative information about nodule to nodule spatial relationships than previous approaches. Future application of the method, and the data it generates, could inform computational models to investigate more specific hypotheses regarding self-organisation mechanisms and pattern formation *in vivo*.

Acknowledgements:

All animal work was subject to ethical approval within Trinity College and carried out under licence (to RR and CS) by the Health Products Regulatory Authority. Thanks to Dermot McMurrough with assistance from Jesko Zimmerman at Trinity College for writing the code to calculate proximity data nearest neighbour distances (NearestTable.py). Thanks to Prof Celia Holland for advice on statistical analysis.

Author's contributions:

Conception and design: RR., CS. and PM. Acquisition of data: RR., and CS. Analysis and interpretation: all authors. Writing and revising the article: all authors. Final approval for publication: all authors.

Conflict of Interest : We declare no conflict of interests

Funding: This work was supported by Trinity College (RR and PM) and an Irish Research Council Postgraduate Studentship (CS).

Ethical Approval: Mice were housed and bred at the Comparative Medicine Unit under accreditation from the Health Products Regulatory Agency (HPRA), Ireland. All animal work was carried out under personal licence from the HPRA. Procedures are approved by the Trinity College Research Ethics Committee where required (all procedures here are covered by licence and no additional ethical approval was required).

References:

Ahrens, P.B., Solursh, M., Reiter, R.S., 1977. Stage-related capacity for limb chondrogenesis in cell culture. Dev Biol 60, 69-82.

Bhat, R., Glimm, T., Linde-Medina, M., Cui, C., Newman, S.A., 2019. Synchronization of Hes1 oscillations coordinates and refines condensation formation and patterning of the avian limb skeleton. Mech Dev 156, 41-54.

Bobick, B.E., Alexander, P.G., Tuan, R.S., 2014. High efficiency transfection of embryonic limb mesenchyme with plasmid DNA using square wave pulse electroporation and sucrose buffer. BioTechniques 56, 85-89.

Bobick, B.E., Chen, F.H., Le, A.M., Tuan, R.S., 2009. Regulation of the chondrogenic phenotype in culture. Birth Defects Res C Embryo Today 87, 351-371.

Brady, K., Dickinson, S.C., Guillot, P.V., Polak, J., Blom, A.W., Kafienah, W., Hollander, A.P., 2014. Human fetal and adult bone marrow-derived mesenchymal stem cells use different signaling pathways for the initiation of chondrogenesis. Stem Cells Dev 23, 541-554.

Butterfield, N.C., Qian, C., Logan, M.P.O., 2017. Pitx1 determines characteristic hindlimb morphologies in cartilage micromass culture. PLoS One 12, e0180453.

Carlberg, A.L., Pucci, B., Rallapalli, R., Tuan, R.S., Hall, D.J., 2001. Efficient chondrogenic differentiation of mesenchymal cells in micromass culture by retroviral gene transfer of BMP-2. Differentiation 67, 128-138.

Christley, S., Alber, M.S., Newman, S.A., 2007. Patterns of mesenchymal condensation in a multiscale, discrete stochastic model. PLoS computational biology 3, e76.

Cunze, S., Kochmann, J., Kuhn, T., Frank, R., Dorge, D.D., Klimpel, S., 2018. Spatial and temporal patterns of human Puumala virus (PUUV) infections in Germany. PeerJ 6, e4255.

Day, T.F., Guo, X., Garrett-Beal, L., Yang, Y., 2005. Wnt/beta-catenin signaling in mesenchymal progenitors controls osteoblast and chondrocyte differentiation during vertebrate skeletogenesis. Dev Cell 8, 739-750.

Delgado, I., Torres, M., 2016. Gradients, waves and timers, an overview of limb patterning models. Semin Cell Dev Biol 49, 109-115.

Duke, P.J., Montufar-Solis, D., Hamazaki, T., Sato, A., 1998. Clinorotation reduces number, but not size, of cartilaginous nodules formed in micromass cultures of mouse limbbud cells. Advances in space research : the official journal of the Committee on Space Research (COSPAR) 21, 1065-1072.

Duprez, D., Bell, E.J., Richardson, M.K., Archer, C.W., Wolpert, L., Brickell, P.M., Francis-West, P.H., 1996. Overexpression of BMP-2 and BMP-4 alters the size and shape of developing skeletal elements in the chick limb. Mech Dev 57, 145-157.

Ferrer-Vaquer, A., Piliszek, A., Tian, G., Aho, R.J., Dufort, D., Hadjantonakis, A.K., 2010. A sensitive and bright single-cell resolution live imaging reporter of Wnt/ß-catenin signaling in the mouse. BMC Dev Biol 10, 121.

Francis-West, P.H., Abdelfattah, A., Chen, P., Allen, C., Parish, J., Ladher, R., Allen, S., MacPherson, S., Luyten, F.P., Archer, C.W., 1999. Mechanisms of GDF-5 action during skeletal development. Development 126, 1305-1315.

Glimm, T., Bhat, R., Newman, S.A., 2020. Multiscale modeling of vertebrate limb development. Wiley Interdiscip Rev Syst Biol Med 12, e1485.

Green, J.B., Sharpe, J., 2015. Positional information and reaction-diffusion: two big ideas in developmental biology combine. Development 142, 1203-1211.

Guo, X., Day, T.F., Jiang, X., Garrett-Beal, L., Topol, L., Yang, Y., 2004. Wnt/beta-catenin signaling is sufficient and necessary for synovial joint formation. Genes Dev 18, 2404-2417.

Hartmann, C., Tabin, C.J., 2000. Dual roles of Wnt signaling during chondrogenesis in the chicken limb. Development 127, 3141-3159.

Hartmann, C., Tabin, C.J., 2001. Wnt-14 plays a pivotal role in inducing synovial joint formation in the developing appendicular skeleton. Cell 104, 341-351.

Juhasz, T., Matta, C., Somogyi, C., Katona, E., Takacs, R., Soha, R.F., Szabo, I.A., Cserhati, C., Szody, R., Karacsonyi, Z., Bako, E., Gergely, P., Zakany, R., 2014. Mechanical loading stimulates chondrogenesis via the PKA/CREB-Sox9 and PP2A pathways in chicken micromass cultures. Cell Signal 26, 468-482.

Klumpers, D.D., Smit, T.H., Mooney, D.J., 2015. The effect of growth-mimicking continuous strain on the early stages of skeletal development in micromass culture. PLoS One 10, e0124948.

Kondo, S., Miura, T., 2010. Reaction-diffusion model as a framework for understanding biological pattern formation. Science 329, 1616-1620.

Krause, C., Guzman, A., Knaus, P., 2011. Noggin. Int J Biochem Cell Biol 43, 478-481.

Long, F., Ornitz, D.M., 2013. Development of the endochondral skeleton. Cold Spring Harb Perspect Biol 5, a008334.

Marcon, L., Diego, X., Sharpe, J., Müller, P., 2016. High-throughput mathematical analysis identifies Turing networks for patterning with equally diffusing signals. eLife 5.

Maretto, S., Cordenonsi, M., Dupont, S., Braghetta, P., Broccoli, V., Hassan, A.B., Volpin, D., Bressan, G.M., Piccolo, S., 2003. Mapping Wnt/beta-catenin signaling during mouse development and in colorectal tumors. Proc Natl Acad Sci U S A 100, 3299-3304.

Mello, M.A., Tuan, R.S., 1999. High density micromass cultures of embryonic limb bud mesenchymal cells: an in vitro model of endochondral skeletal development. In vitro cellular & developmental biology. Animal 35, 262-269.

Mello, M.A., Tuan, R.S., 2006. Effects of TGF-beta1 and triiodothyronine on cartilage maturation: in vitro analysis using long-term high-density micromass cultures of chick embryonic limb mesenchymal cells. J Orthop Res 24, 2095-2105.

Mendes, L.F., Tam, W.L., Chai, Y.C., Geris, L., Luyten, F.P., Roberts, S.J., 2016. Combinatorial Analysis of Growth Factors Reveals the Contribution of Bone Morphogenetic Proteins to Chondrogenic Differentiation of Human Periosteal Cells. Tissue Eng Part C Methods 22, 473-486.

Miao, Q., Yuan, Y.J., Luo, G.M., Wei, C.H., Rao, Y.Q., Gong, Y.H., Zhang, L., Shao, J., Dong, Y.K., 2016. [Study on ecological suitability of Gardenia jasminoides based on ArcGIS and Maxent model]. Zhongguo Zhong yao za zhi = Zhongguo zhongyao zazhi = China journal of Chinese materia medica 41, 3181-3185.

Miura, T., Komori, M., Shiota, K., 2000. A novel method for analysis of the periodicity of chondrogenic patterns in limb bud cell culture: correlation of in vitro pattern formation with theoretical models. Anat Embryol (Berl) 201, 419-428.

Miura, T., Shiota, K., 2000a. Extracellular matrix environment influences chondrogenic pattern formation in limb bud micromass culture: experimental verification of theoretical models. Anat Rec 258, 100-107.

Miura, T., Shiota, K., 2000b. TGFbeta2 acts as an "activator" molecule in reaction-diffusion model and is involved in cell sorting phenomenon in mouse limb micromass culture. Dev Dyn 217, 241-249.

Newman, G.D., Smith, A.L., Brody, S.D., 2017. Repurposing Vacant Land through Landscape Connectivity. Landscape journal 36, 37-57.

Norrie, J.L., Lewandowski, J.P., Bouldin, C.M., Amarnath, S., Li, Q., Vokes, M.S., Ehrlich, L.I.R., Harfe, B.D., Vokes, S.A., 2014. Dynamics of BMP signaling in limb bud mesenchyme and polydactyly. Dev Biol 393, 270-281.

Nyakarahuka, L., Ayebare, S., Mosomtai, G., Kankya, C., Lutwama, J., Mwiine, F.N., Skjerve, E., 2017. Ecological Niche Modeling for Filoviruses: A Risk Map for Ebola and Marburg Virus Disease Outbreaks in Uganda. PLoS currents 9.

Olanrewaju, O.E., Adepoju, K.A., 2017. Geospatial Assessment of Cholera in a Rapidly Urbanizing Environment. Journal of environmental and public health 2017, 6847376.

Onodera, K., Takahashi, I., Sasano, Y., Bae, J.W., Mitani, H., Kagayama, M., Mitani, H., 2005. Stepwise mechanical stretching inhibits chondrogenesis through cell-matrix adhesion mediated by integrins in embryonic rat limb-bud mesenchymal cells. Eur J Cell Biol 84, 45-58.

Raspopovic, J., Marcon, L., Russo, L., Sharpe, J., 2014. Modeling digits. Digit patterning is controlled by a Bmp-Sox9-Wnt Turing network modulated by morphogen gradients. Science 345, 566-570.

Ray, A., Singh, P.N., Sohaskey, M.L., Harland, R.M., Bandyopadhyay, A., 2015. Precise spatial restriction of BMP signaling is essential for articular cartilage differentiation. Development 142, 1169-1179.

Rolfe, R.A., Shea, C.A., Singh, P.N.P., Bandyopadhyay, A., Murphy, P., 2018. Investigating the mechanistic basis of biomechanical input controlling skeletal development: exploring the interplay with Wnt signalling at the joint. Philos Trans R Soc Lond B Biol Sci 373.

Rudnicki, J.A., Brown, A.M., 1997. Inhibition of chondrogenesis by Wnt gene expression in vivo and in vitro. Dev Biol 185, 104-118.

Saha, A., Rolfe, R., Carroll, S., Kelly, D.J., Murphy, P., 2017. Chondrogenesis of embryonic limb bud cells in micromass culture progresses rapidly to hypertrophy and is modulated by hydrostatic pressure. Cell Tissue Res 368, 47-59.

Seemann, P., Schwappacher, R., Kjaer, K.W., Krakow, D., Lehmann, K., Dawson, K., Stricker, S., Pohl, J., Ploger, F., Staub, E., Nickel, J., Sebald, W., Knaus, P., Mundlos, S., 2005. Activating and deactivating mutations in the receptor interaction site of GDF5 cause symphalangism or brachydactyly type A2. J Clin Invest 115, 2373-2381.

Singh, P.N.P., Shea, C., Sonker, S.K., Rolfe, R., Ray, A., Kumar, S., Gupta, P., Murphy, P., Bandyopadhyay, A., 2018. Precise spatial restriction of BMP signaling in developing joints is perturbed upon loss of embryo movement. Development.

Spater, D., Hill, T.P., Gruber, M., Hartmann, C., 2006. Role of canonical Wnt-signalling in joint formation. Eur Cell Mater 12, 71-80.

Summerhurst, K., Stark, M., Sharpe, J., Davidson, D., Murphy, P., 2008. 3D representation of Wnt and Frizzled gene expression patterns in the mouse embryo at embryonic day 11.5 (Ts19). Gene Expr Patterns 8, 331-348.

Takacs, R., Matta, C., Somogyi, C., Juhasz, T., Zakany, R., 2013. Comparative analysis of osteogenic/chondrogenic differentiation potential in primary limb bud-derived and C3H10T1/2 cell line-based mouse micromass cultures. Int J Mol Sci 14, 16141-16167.

Zimmerman, L.B., De Jesús-Escobar, J.M., Harland, R.M., 1996. The Spemann organizer signal noggin binds and inactivates bone morphogenetic protein 4. Cell 86, 599-606.

Tables and figures:

Table 1: Custom designed primer sequences used for qRT-PCR expression analysis.

Gene	Ref Sequence	Fwd	Rv
Col2a1	NM_0332263.3	AAGTCACTGAACAACCAGATTGAGA	AAGTGCGAGCAGGGTTCTTG
Sox9	NM_011448.4	CGGCTCCAGCAAGAACAAG	TGCGCCCACACCATGA
Col10a1	NM_009925.4	TGCAATCATGGAGCTCACAGA	CAGAGGAGTAGAGGCCGTTTGA
Ihh	NM_010544.2	CCACCTTCAGTGATGTGCTTATTT	CGATGACCTGGAAAGCTCTCA
Gapdh	NM_008084	TGGCCTCCAAGGAGTAAGAAAC	GGGATAGGGCCTCTCTTGCT

Figure Legends

Figure 1: Methodological pipeline used to analyse the self-organisation pattern of chondrogenic nodules. (a) Original image of whole micromass culture stained with Alcian Blue, (b) 5mm circular cropped region of interest (ROI), boxed region indicating debris, (c) image was 'cleaned' by encircling debris / artefacts and filling the enclosed space (red arrowhead (b-c)). (d-d'') cleaned images split into component channels (d) Red, (d') Green and (d'') Blue. (e) Conversion of Green channel into binarised black (nodules) and white (space between nodules) image. Noise was removed (red arrowhead) and (f) converged nodules were separated (green arrowhead) with watershed function. (g) Encircling of each nodule (minimum particle size of 0.005 μm^2) was performed with the analyse particles function. (h-k) illustration and formulae of how nodule shape and spatial relationship measurements were calculated, (h) circularity (i) solidity, with values closer to 1 indicating a more circular and more solid shape, (j) nodule spacing; illustrative example of the process measuring the distance from one nodule's centre point (red dots) to the nearest centre point of another nodule and (k) nodule proximity; illustrative example of the process measuring the distance between a point on the perimeter of a given nodule (green dot) and the closest point on the perimeter of neighbouring nodule. Scale bar, 1mm

Figure 2: Profile of chondrogenesis of primary E11.5 limb bud cells and establishment of geometric characteristics of chondrogenic nodules. (a-a'') Tracking of individual condensations in the same micromass culture over time shows that cell condensations appear and grow with edges coming closer together. (a) coloured pinpoints trace the appearance of cell condensations on live images over the time frame indicated, (a') overlay of images with

clustering of pinpoints, (a'') clustered pinpoints overlaid on the same culture at 144 hrs, Alcian Blue stained and thresholded. (b) Chondrogenic profile of E11.5 limb bud micromass cultures stained with Alcian Blue showing appearance of chondrogenic nodules over time. Quantification of (c) nodule number, (d) % area covered by nodules, (e) average nodule size (x1000μm^2); shape parameters (f) circularity and (g) solidity; and nodule to nodule spatial relationships (h) nodule spacing (μm) and (i) nodule proximity (μm). Y-axes are the same for f & g, and h and i. Data is shown as mean ± SEM. # p≤0.01* p≤0.05, ** p≤0.001, *** p≤0.0001. Scale bar 1mm

Figure 3: Profile of chondrogenesis in E11.5 mouse limb bud cell micromass cultures is altered following the addition of BMP and Wnt signaling molecules. (a) Micromass cultures in growth media (GM) or (b) in the presence of BMP2 (100ng/ml) or (c) WNT3A (200ng/ml) over time, stained with Alcian Blue. Scale bar 1mm. (d – i) Geometric analysis showing (d) nodule number, (e); average nodule size (μm^2), (f) % area covered by nodules, (g) circularity and nodule to nodule spatial relationships (h) nodule spacing (μm) and (i) nodule proximity (μm). Changes in chondrogenic *(Col2a1*) (j) and hypertrophic (*Ihh*) (k) marker gene expression in micromass culture in growth media (GM) or in the presence of BMP2 (100ng/ml) or WNT3A (200ng/ml) over time. Expression level in each sample was normalised to *Gapdh* and shown relative to expression at 0 hours, set to 1. Data are mean ± SEM. Blue boxes: growth media, Orange boxes: +BMP2(100ng/ml) group, Yellow boxes: +WNT3A(200ng/ml) group. Black lines indicate significant difference across groups, yellow lines indicate significant difference within the WNT3A group. #p≤0.01 *p≤0.05, **p≤0.001, ***p≤0.0001

Figure 4: Titration of chondrogenic signaling molecules adjusts the equilibrium in condensation organisation in micromass culture. (a) Proportion of chondrogenic nodules relative to GM at 144 hrs for WNT3A addition (yellow circles; conc. as indicated on left y axis; 200ng/ml,100ng/ml and 50ng/ml), Noggin (grey circles; conc. as indicated on right y axis, 100ng/ml, 50ng/ml and 10ng/ml) and BMP2 (orange circles; conc. as indicated on right y axis, 100ng/ml, 50ng/ml and 10ng/ml) (b) % area covered by nodules and (b') average nodule size (x1000μm^2), (c) nodule spacing (μm), (d) nodule proximity (μm). Data are mean ± SEM. Blue boxes: growth media, Orange: BMP2 groups, Grey: NOG, Yellow: WNT3A groups. Concentrations of added BMP2, NOG and WNT3A for all graphs are shown against the x-axis of d. The y-axes on the right of c and d show an expanded scale needed to represent the data following addition of 200ng/ml WNT3A. (b-d) Black lines indicate significant difference

comparing additive with GM; orange, grey and yellow lines indicate significant difference within the BMP2, NOG and WNT3A treatment groups respectively *p≤0.05, **p≤0.001, ***p≤0.0001. (e-e’’’’) profile plots of selected nodule geometric parameters (showing mean values) as BMP2, WNT3A, and Noggin signaling molecule concentrations increase. Upward trends are shown in red, downward trends in blue. Nodule spacing on addition of WNT3A is not shown but indicated as “irregular”, as shown by the large variability in the graphs (4c, d) and analysis of individual cultures (Supplementary Fig 5).

Figure 1

Click here to access/download;Figure;Fig 1_FINAL.tiff

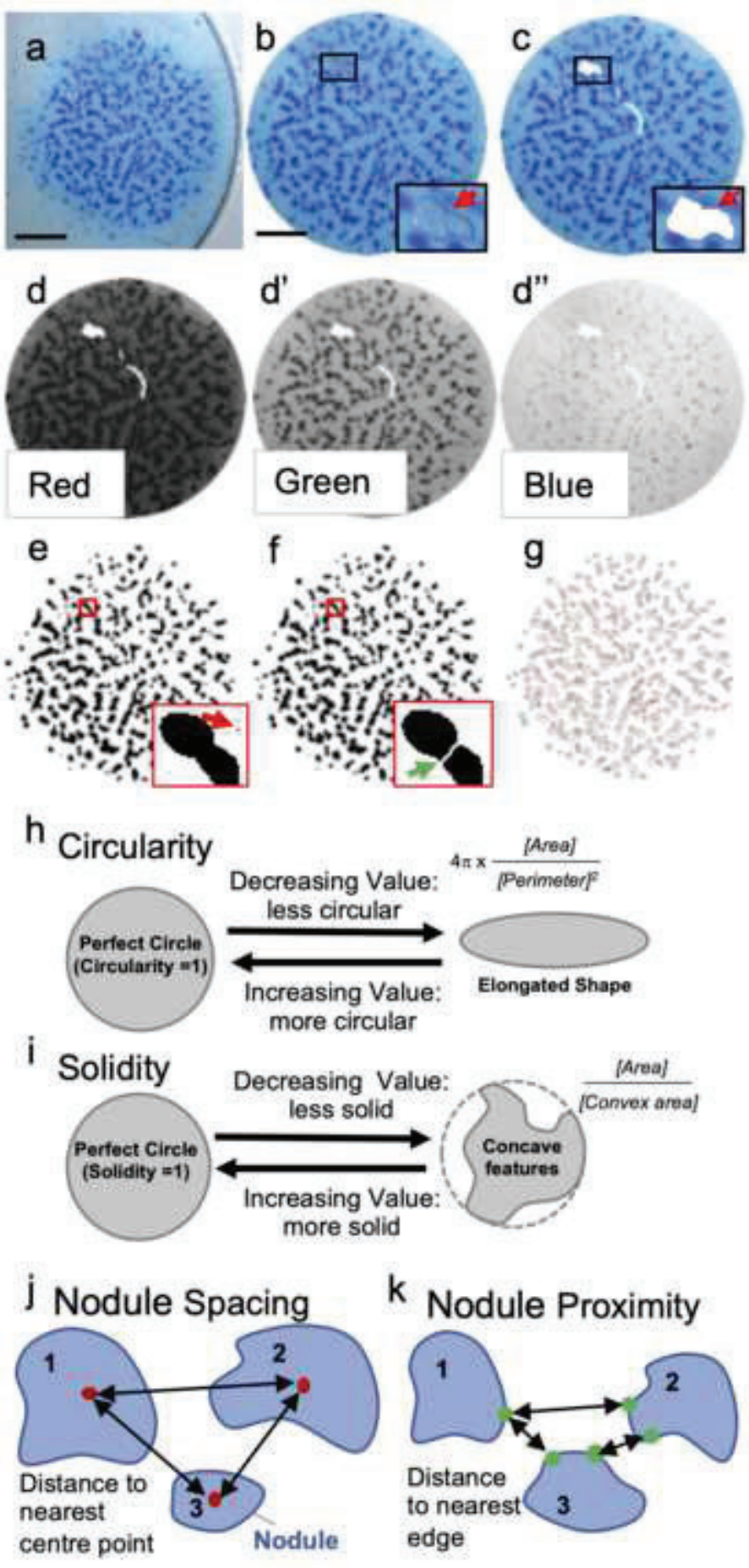

Figure 2 adjusted

Click here to access/download;Figure;Fig 2_FINAL_updated.tiff

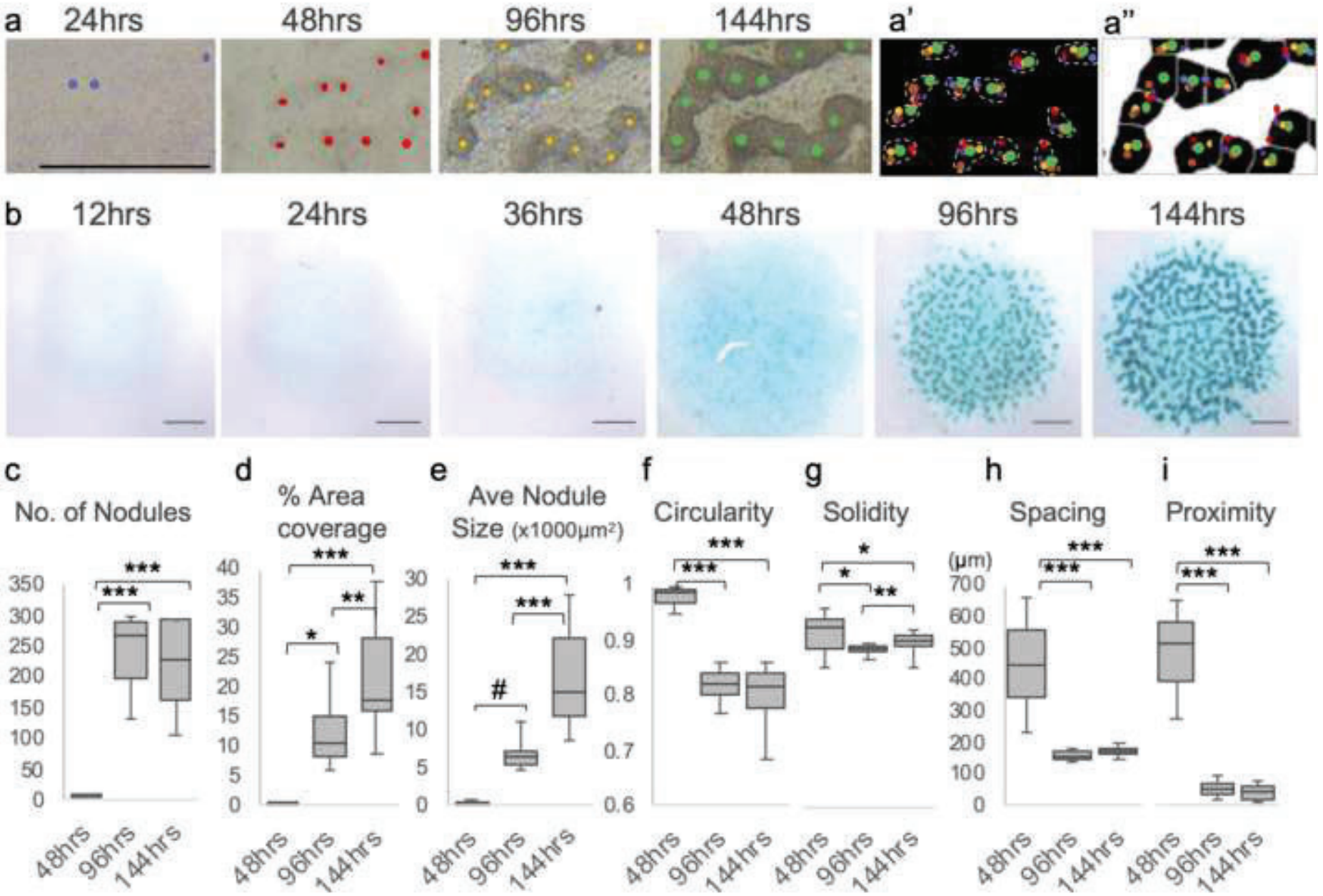

Figure 3 adjusted

Click here to access/download;Figure;Fig 3_FINAL_updated.tiff

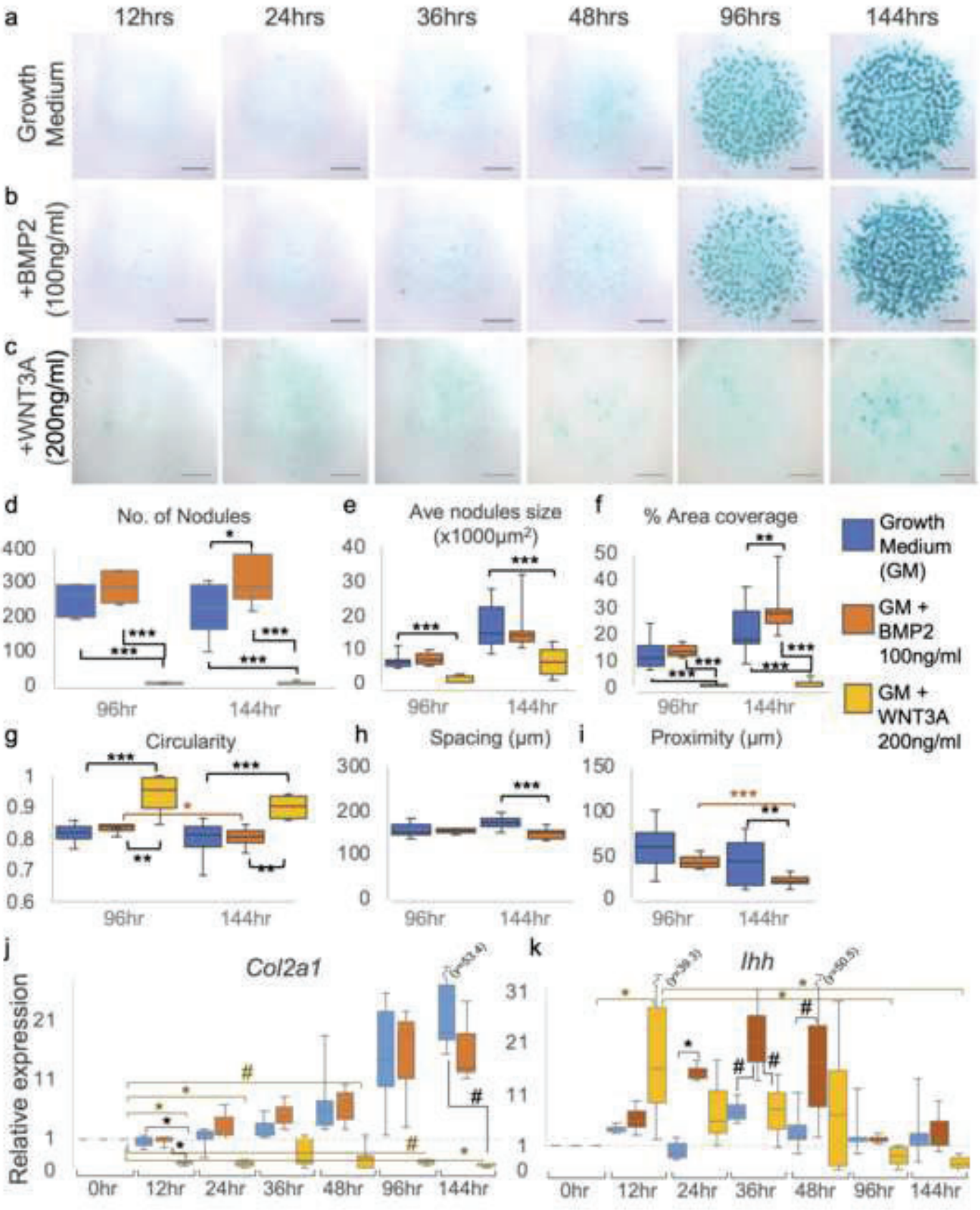

Figure 4

Click here to access/download;Figure;Fig 4_FINAL.tiff

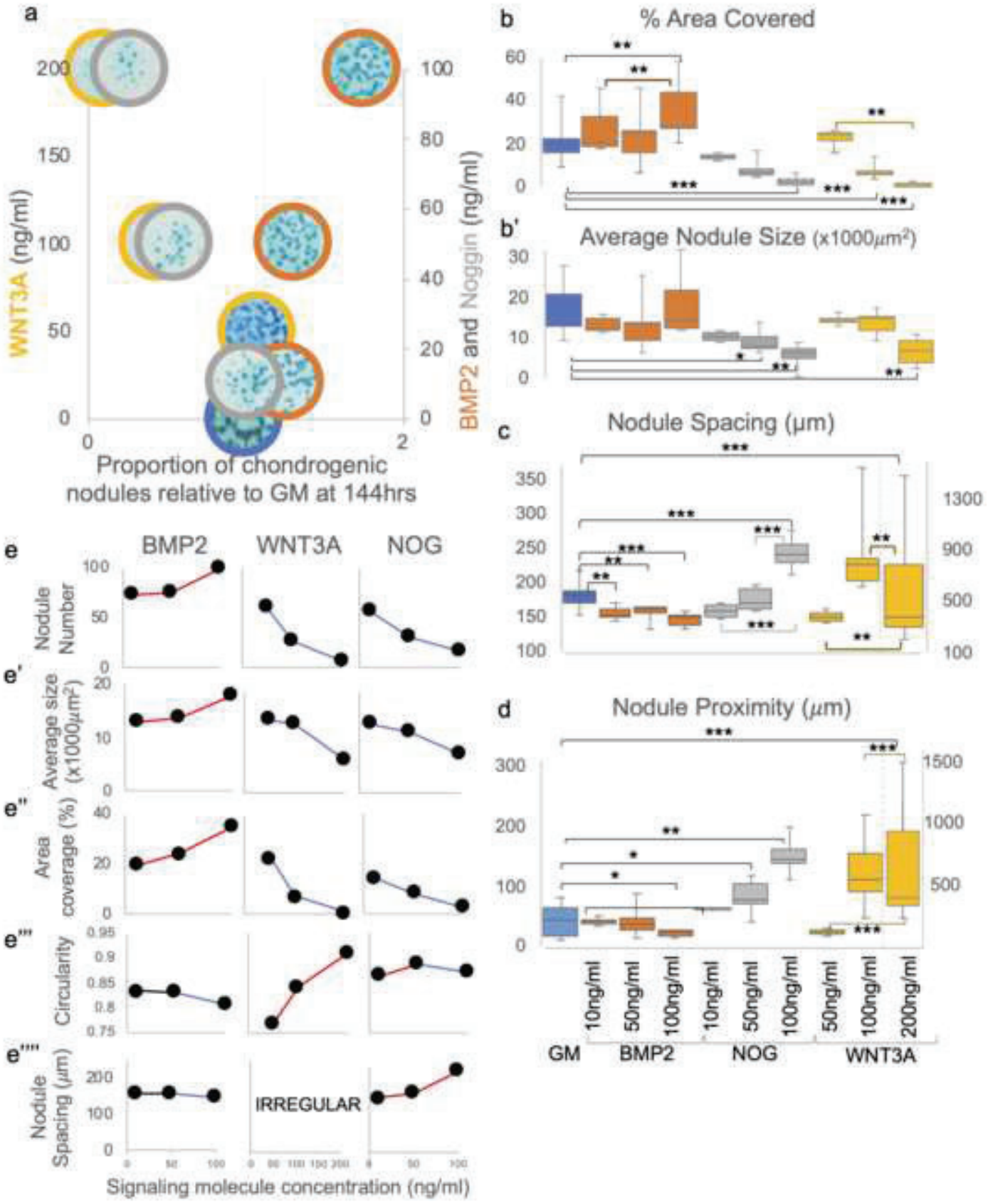

Supplementary Material 1

Supplementary Material 2